High-energy γ rays resulting from low-energy nuclear reactions in light nuclei

Paul B. Rose Jr. and Anna S. Erickson*

Georgia Institute of Technology, Nuclear and Radiological Engineering, G.W. Woodruff School of Mechanical Engineering, 770 State St., Atlanta, Georgia 30332, USA

(Received 9 January 2018; published 7 June 2018)

Products resulting from 3.02 MeV deuterons incident on a natural boron target have been investigated by way of γ-ray spectroscopy and activation analysis. This study uses observed γ rays and cascades to deduce the populated states from the reaction products. Die-away measurements are included to investigate the built-up activation from the target and compared with tabulated half-lives to further understand the plethora of reactions taking place. Many of the observed γ rays, such as 15.1 MeV, result from the formation of excited states of ^{12}C, while others are secondary and tertiary processes from α breakup resulting in ^{8}Be.

DOI: 10.1103/PhysRevC.97.064305

I. INTRODUCTION

Population of the 15.1 MeV (1^+) state of ^{12}C has been reported by multiple investigations since it was first discovered by Johnson [1]. Subsequent studies aimed to refine the understanding of excited levels in light nuclei and to quantify the cross sections for achieving this state with light ions [2–5]. Almqvist *et al.* [6] and Kuan *et al.* [5] investigated the γ-ray branching ratio of the 15.1 MeV state of ^{12}C and determined the deexcitation to the ground state 97% of the time resulting in a 15.1 MeV γ-ray emission ($M1$) and 3% to the first-excited state. The 15.1 MeV excited state of ^{12}C is the $T_z = 0$ isobaric triplet with relation to the ground states of ^{12}B and ^{12}N. In fact, the excited carbon nucleus contains enough energy to break up directly into three α particles, with a threshold energy of 7.275 MeV, or a ^{8}Be nucleus and an α particle [7]. This breakup is forbidden by the isobaric spin selection rules implying a strong preferential deexcitation by γ-ray emission instead.

The studies in Refs. [2–6] were carried out by using a range of accelerated ions (protons, deuterons, tritons, and α particles) impinging on light nuclei as a function of ion kinetic energy. Many of these reactions will leave the resulting nuclei in an excited state independent of kinetic energy while others are threshold reactions. One such reaction is the ^{11}B-deuteron reaction, which usually results in the emission of neutrons to produce excited states of ^{12}C and subsequent γ rays. The incident deuteron must be accelerated to a minimum of 1.633 MeV to produce the desired 15.1 MeV excited state; otherwise lower excited states are populated including the Hoyle state at 7.6 MeV, which preferentially decays through the three α or $^{8}\mathrm{Be} + \alpha$ processes [8].

The cross section for the $^{11}\mathrm{B}(d,n-\gamma)^{12}\mathrm{C}_{\gamma_{15.1\ \mathrm{MeV}}}$ reaction has been studied by multiple groups [4,5,9–11] by analyzing the resulting neutrons and γ rays. Those studies were carried out using NaI or BGO detectors which have poor energy resolution relative to other scintillators such as LaBr and CsI. Their findings on the magnitude of the 15.1 MeV excited-state cross section vary significantly. However, all three studies found a resonance centered at $E_d = 3.08$ MeV for populating the 15.1 MeV excited state. They collectively indicate other γ-ray emissions detected in their experiments which were not explored. These γ rays could be the result of unknown states or secondary and tertiary nuclear reactions taking place from the products.

Taddeucci *et al.* [9] explored this nuclear reaction by varying the energy of the impinging deuterons from 3.0 to 7.4 MeV on enriched, 97.15%, ^{11}B targets of various thicknesses. The resulting γ rays were studied with a 10×10 cm^2 BGO detector, and the neutrons were detected with NE-213 liquid scintillators. The detectors were placed at 180 degrees relative to each other with the boron target in-between, affording them the opportunity to perform time-of-flight gating and spectroscopy on the observed radiation. One important finding was that many of the observed γ rays below the 15.1 MeV emission nearly vanished when using a time gating of 32 ns to isolate the prompt γ rays. This poses a question as to the origin of these emissions. Nuclei excited to these energies are generally highly unstable and decay with a half-life in femtoseconds or less. The longevity of these emissions suggests subsequent nuclear reactions or unknown quasi-long-lived states may be present.

Monoenergetic, higher-energy γ rays could be of great use when high γ-ray penetrability [12] or photofission [13] is of interest. One example is in nuclear security applications where the γ rays could be used to probe through shielding to uncover illicit special nuclear material (SNM) in transit [14–16]. The γ rays could penetrate the potential shielding masking the hidden threat and any photons above 5 MeV could induce photofission in the SNM.

The goal of the work presented in this paper aims to determine the exact energies and potential origins of the observed γ rays from the $^{11}\mathrm{B}(d,n\text{-}\gamma)^{12}\mathrm{C}$ reaction. Understanding the root of these γ-ray emissions will assist in the design of new discrete-energy γ-ray sources for nuclear security applications. For practicality of these γ rays in nuclear security, we

*erickson@gatech.edu

TABLE I. Initial nuclear reactions and abundance greater than 0.5% resulting from 3.02 MeV deuterons incident on natural boron as calculated by GEANT4. Secondary reactions are omitted from the list.

Reaction	Relative yield	Q value
$d + {}^{11}\mathrm{B} \rightarrow n + 3\alpha$	34.20%	6.46 MeV
$d + {}^{11}\mathrm{B} \rightarrow \gamma + n + {}^{12}\mathrm{C}$	25.68%	13.73 MeV
$d + {}^{11}\mathrm{B} \rightarrow \alpha + {}^{9}\mathrm{Be}$	8.94%	8.03 MeV
$d + {}^{10}\mathrm{B} \rightarrow \gamma + p + {}^{11}\mathrm{B}$	7.17%	9.23 MeV
$d + {}^{10}\mathrm{B} \rightarrow \gamma + n + {}^{11}\mathrm{C}$	6.87%	6.46 MeV
$d + {}^{11}\mathrm{B} \rightarrow d' + {}^{11}\mathrm{B}$	5.17%	
$d + {}^{11}\mathrm{B} \rightarrow \gamma + p + {}^{12}\mathrm{B}$	3.52%	1.15 MeV
$d + {}^{10}\mathrm{B} \rightarrow d + {}^{10}\mathrm{B}$	2.28%	
$d + {}^{11}\mathrm{B} \rightarrow p + {}^{12}\mathrm{B}$	1.39%	1.15 MeV
$d + {}^{11}\mathrm{B} \rightarrow n + {}^{12}\mathrm{C}$	1.19%	13.73 MeV
$d + {}^{10}\mathrm{B} \rightarrow p + {}^{11}\mathrm{B}$	0.99%	9.23 MeV
$d + {}^{10}\mathrm{B} \rightarrow n + {}^{11}\mathrm{C}$	0.92%	6.46 MeV
$d + {}^{10}\mathrm{B} \rightarrow 3\alpha$	0.81%	17.91 MeV
$d + {}^{10}\mathrm{B} \rightarrow \gamma + d' + {}^{10}\mathrm{B}$	0.67%	

investigated the products of the reaction both computationally with GEANT4 simulations as well as experimentally using a high-purity germanium (HPGe) detector.

II. SIMULATED REACTIONS

We begin by investigating which nuclear reactions are energetically possible by employing Monte Carlo-based simulations. For our investigation, we chose to use GEANT4 [17,18], a simulation toolkit with a focus on particle propagation and interactions through matter. This toolkit gives the ability to simulate particle interactions based on cross sections or physics models. We chose to use physics models, such as Bertini, for nuclear interactions because it has been established that sufficient cross-section information and excited-state branching ratios for this reaction do not exist [19]. The main physics lists used here are G4HadronElasticPhysicsHP, G4HadronPhysicsFTFP_BERT_HP, G4IonElasticPhysics, G4IonPhysics, G4EmStandardPhysics, and GammaPhysics.

Our simulation uses a 2-mm-thick natural boron target surrounded by vacuum. The target is bombarded with a 3.02 MeV deuteron beam to mimic our experiment. GEANT4 provides access to the processes taking place at every level, so we are able to tally and track the entire cascade of nuclear reactions taking place in the target as well as the energy distribution of particles produced. We simulated 10^9 deuterons incident on the target which yielded a total of 687 possible nuclear reactions. A summary of these reactions can be found in Table I, where we omit reactions occurring less than 0.5% of the total.

It is important to note that the Q values presented here are a balance of the kinetic energy before and after the collision. However, the nuclear excitation energy of some levels is not included because there are not sufficient deexcitation data forcing GEANT4 to process them as nucleon decays [20]. For example, the Q value for the $^{11}\mathrm{B}(d,n\text{-}\gamma)^{12}\mathrm{C}$ is calculated by GEANT4 as 13.73 MeV, which is not enough to populate the 15.1 MeV state of $^{12}\mathrm{C}$. When analytically calculating the Q value and accounting for the possible kinetic energy from the deuteron, the Q_{excited} is calculated to be 16.28 MeV, overcoming the threshold and reaching the 15.1 MeV excited state. This leads us to conclude the second reaction listed in Table I, $^{11}\mathrm{B}(d,n\gamma)^{12}\mathrm{C}$, only includes γ rays from states below the desired 15.1 MeV state.

TABLE II. Summary of particles generated per 10^9 incident deuterons and kinetic-energy range as calculated by GEANT4 at the time of emission. Percent yield is the number of particles generated divided by the number of incident deuterons multiplied by 100%.

Product	% yield	Avg. energy	Energy range
$^{10}\mathrm{B}$	13.679%	611.61 keV	0.009 eV → 20.545 MeV
$^{11}\mathrm{B}$	60.435%	635.07 keV	0.002 eV → 22.289 MeV
$^{12}\mathrm{B}$	4.985%	636.23 keV	159.43 eV → 10.236 MeV
$^{9}\mathrm{B}$	0.001%	1.15 MeV	2.775 keV → 3.513 MeV
$^{10}\mathrm{Be}$	0.145%	1.60 MeV	70.28 eV → 12.991 MeV
$^{11}\mathrm{Be}$	0.017%	1.32 MeV	256.54 keV → 3.809 MeV
$^{7}\mathrm{Be}$	0.070%	596.25 keV	67.268 eV → 11.295 MeV
$^{8}\mathrm{Be}$	0.042%	4.09 MeV	661.48 eV → 12.535 MeV
$^{9}\mathrm{Be}$	9.253%	3.55 MeV	121.81 eV → 19.993 MeV
$^{10}\mathrm{C}$	0.004%	946.02 keV	70.393 keV → 4.4406 MeV
$^{11}\mathrm{C}$	7.945%	749.43 keV	5.025 eV → 15.736 MeV
$^{12}\mathrm{C}$	27.688%	961.08 keV	75.23 eV → 22.132 MeV
$^{13}\mathrm{C}$	0.596%	1.78 MeV	129.86 eV → 14.691 MeV
$^{14}\mathrm{C}$	0.463%	1.58 MeV	7.542 keV → 15.097 MeV
$^{3}\mathrm{He}$	0.006%	3.98 MeV	36.39 keV → 14.749 MeV
$^{6}\mathrm{He}$	0.001%	2.60 MeV	28.845 keV → 15.411 MeV
$^{6}\mathrm{Li}$	0.004%	4.43 MeV	254.21 eV → 22.014 MeV
$^{7}\mathrm{Li}$	2.732%	1.69 MeV	65.774 eV → 17.2 MeV
$^{8}\mathrm{Li}$	0.181%	2.28 MeV	148.97 eV → 8.607 MeV
$^{13}\mathrm{N}$	0.103%	1.63 MeV	10.873 keV → 13.244 MeV
$^{14}\mathrm{N}$	2.360%	1.59 MeV	18.464 keV → 15.28 MeV
$^{15}\mathrm{N}$	0.003%	3.14 MeV	4.152 keV → 14.997 MeV
$^{16}\mathrm{O}$	0.002%	2.60 MeV	71.161 keV → 16.613 MeV
$^{17}\mathrm{O}$	0.002%	2.83 MeV	121.98 keV → 16.175 MeV
α	123.732%	2.68 MeV	1.129 eV → 38.425 MeV
d	8.596%	2.23 MeV	1.090 keV → 25.033 MeV
n	78.545%	6.42 MeV	3.654 eV → 30.857 MeV
p	14.672%	4.86 MeV	177.12 eV → 26.038 MeV
t	0.560%	2.57 MeV	3.442 eV → 31.807 MeV

The first three reactions listed in Table I are competing processes. We do not claim validity of these yields, but they give an estimate to compare with observed experimental data. One important result is the abundance of the $^{11}\mathrm{B}(d,n)3\alpha$, occurring nearly 34% of the time from incident deuterons. This is the most prominent nuclear reaction occurring in the simulations, which does not directly add to the desired high energy γ-ray output. However, the tabulated relative yield of the three-α reaction could be the summed total of that reaction and the $^{11}\mathrm{B}(d,n\gamma)^{12}\mathrm{C}$ where the γ ray is the desired 15.1 MeV. The next most probable reaction is the desired $^{11}\mathrm{B}(d,n\gamma)^{12}\mathrm{C}$ reaction and the $^{11}\mathrm{B}(d,\alpha)^{9}\mathrm{Be}$ reaction resulting in a 1.68 MeV γ ray. The resulting particles generated from these reactions can be found in Table II.

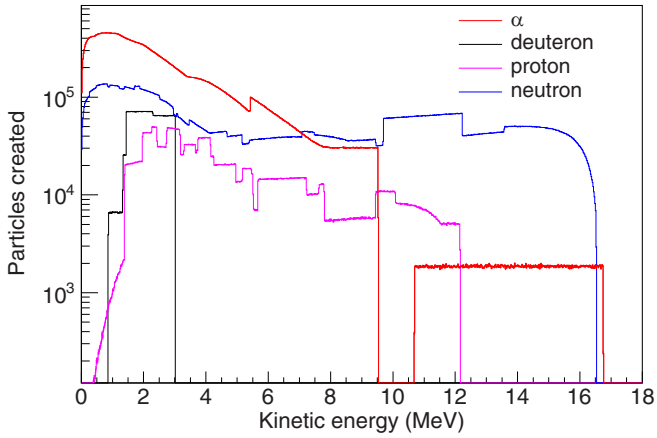

FIG. 1. Kinetic energies of some of the reaction products at the instant of emission including stripping reactions. As the particles propagate through the target material they slow down and/or cause other reactions to occur.

In Table II we omit the γ-ray production from this list due to the lack of tabulated emission intensities, branching ratios, and even available energy states in some cases. This is a known limitation [20] of available nuclear data which we hope to explore experimentally. Table II includes products from all reactions including those from secondary and tertiary products leading to nuclide buildup above carbon. This list represents approximately one second of deuteron bombardment. The kinetic energy of each particle at the time of generation is tabulated to build energy histograms as seen in Fig. 1.

The noncontinuous nature of the distributions is due to the tally at time of origin and includes stripping reactions. All of these particles are generated inside the boron target and many go on to create additional nuclear reactions. The ranges of the charged particles are generally small inside the target, but many do make it out to the aluminum target holder and endcap. Here, we can see that GEANT4 is accounting for thresholds of emissions presented as step-like functions. The energy of an emitted particle can be continuous between a minimum threshold and a threshold of a different reaction. There is a significant amount of particles generated inside the target itself that can spawn other reactions that go on to yield γ rays. Generally, this will take longer than 32 ns, suggested by Taddeucci, from the time of the ^{12}C prompt γ emissions suggesting a possible source of intermediate-energy γ rays.

This simulation analysis was extended to include most prominent material surrounding the boron target to investigate the associated reactions as described in the experimental setup section. The tabulated results of these simulations and the full output of the target simulations can be found in Rose [21].

III. EXPERIMENTAL SETUP

A. Source of discrete-energy photons

Experimentally, we employ a compact linear accelerator to impinge deuterons into 2-mm-thick natural boron $^{\text{nat.}}$B target commercially available from Goodfellow USA. The reaction is driven by a modified LANSAR Model DL-3 radio frequency quadrupole accelerator manufactured by Accsys Technology Inc., which produces a 3.02 MeV d^+ beam with versatile pulse rates and lengths.

This source produces deuterons with kinetic energy close to the broadened 3.08 MeV resonance [4,5,9] of populating the 15.1 MeV (1^+) state of ^{12}C. The source also differs from previous works in the choice of target composition and dimensions. We are using a "thick" (2 mm) natural boron with an approximate isotopic abundance of ^{10}B and ^{11}B being 19.9% and 80.1%, respectively. The presence of ^{10}B expands the possibilities of potential nuclear reactions beyond those associated with just ^{11}B. It is crucial to understand the exact energies and relative abundances of the γ rays resulting from the nuclear reaction in the target as well as other interactions in the experimental setup. Further complicating the potential reaction list, the boron target is fixed to the inside of an aluminum endcap to seal the vacuum of the accelerator.

Since both of the most common reactions in Table I produce neutrons, we applied a filter consisting of a 50.8-cm-thick block of high-density borated polyethylene (HDBP, 5% wt. boron) placed between the source and detectors. This reduces the neutron flux by orders of magnitude while having only minor effects on the higher-energy γ rays of interest. The source is collimated by using a combination of lead, HDPE, and two rows of large concrete blocks with a separation of 2.54 cm. These multiple layers of collimation result in a fan beam spanning the height of a cargo container for potential active interrogation experiments [22]. The copious amounts of shielding and collimation provide a relatively low room-return environment for the detectors placed approximately 9 m from the boron target.

B. High-purity Ge detector system

The detector system employed here was a mobile high-purity germanium detector, HPGe, model GC8021 manufactured by Canberra Industries using a Big-Mac liquid nitrogen cooling system. The detector was modified to operate using a model 2101P-10 transistor reset preamplifier (TRP) instead of a traditional RC preamplifier to reduce dead time in the high-flux accelerator environments. Other design elements were customized to allow the detector to operate comfortably detecting γ rays of up to 20 MeV. The modification to utilize the TRP has one major drawback; the forced resetting is a function of the energy deposition rate in the semiconductor crystal. This means the high-energy photons may be ignored more frequently than the lower-energy photons leading to miscalculation of ratios of the detected photons. This detector is selected to provide the best possible energy resolution of the incident γ rays for identification of the exact γ transitions. Another detector system can be used to calculate relative detection ratios in the future such as a LaBr detector. The HPGe detector was controlled by using a LYNX digital MCA from Canberra Industries to optimize the detectors performance. We used GENIE2K, also from Canberra Industries, to set the MCA parameters and collect data from the detector.

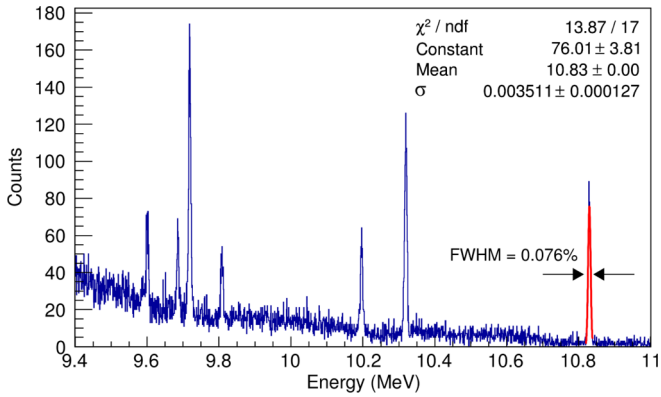

FIG. 2. Example of detector energy resolution at high energies. Here we observe the 10.83 MeV γ ray from thermal neutron capture by ^{14}N. Also shown is the Gaussian fitting and parameters described in the energy-calibration techniques discussion.

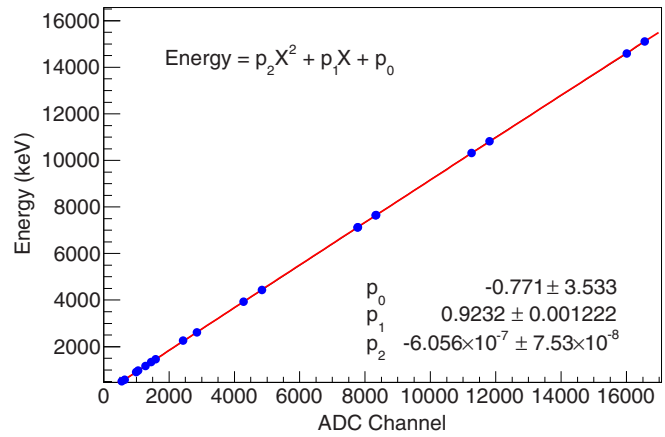

FIG. 3. HPGe energy versus Analog to Digital Conversion CHannel (ADCCH) calibration with polynomial fitting function and errors as calculated by ROOT. The blue points on the plot mark the measured peak centroid and tabulated γ-ray energy. The error on the measured centroids is included but is smaller than the markers used to portray the points.

IV. ENERGY CALIBRATION AND ANALYSIS

Energy calibrations were performed by using a variety of sources including ^{60}Co, PuBe, as well as well-known 0.511, 4.439, and 15.11 MeV lines from the primary nuclear reaction, ^{11}B$(d,n\gamma)^{12}$C. These were supplemented with additional calibration points by using prompt γ rays from neutron capture in ^{56}Fe, spawning 7.631 and 7.645 MeV, and ^{14}N, yielding 10.829 MeV γ rays. These were chosen due to the energy range and ease of generation. For the energy calibration experiment we used a ^{252}Cf source for neutrons placed next to a dewar of liquid nitrogen. We then evacuated the liquid nitrogen and repeated the experiment with just the steel dewar; subtracting the two spectra yields all γ lines related to nitrogen. The iron lines are easily visible from the steel dewar itself. Leveraging the physics of pair production to increase the number of calibration points, we used the full energy deposition and single escape peaks from all three emissions in the energy calibration. The full energy and single escape from the nitrogen capture can been seen in Fig. 2.

These intermediate γ-ray energies are crucial for accurate calibration of the spectrum collected from the beam down to single-digit keV levels, which enables us to determine if they are the result of reactions in the target or surroundings. Unlike the 4.4 MeV γ rays from a PuBe source, there is no Doppler broadening associated with the emission of the selected γ rays because they originate from thermal neutron capture in relatively heavy nuclei. The HPGe detector employed here has an energy resolution of 0.076% at 10.8 MeV. This energy resolution is important to determine the exact energy of unknown γ rays resulting from the deuteron-on-boron reactions. It is difficult to account for deviations from linearity in the detection process without having enough energy calibration points in the range of interest.

A Gaussian fit was applied to each well-resolved peak using ROOT to obtain the peak centroid and associated error to compile a channel versus energy relationship as seen in Fig. 3. To check the fidelity of the calibration, we attempted multiple fitting functions and calculated the known energies, and then calculated the percent error from the fitting relationship.

Semiconductor detectors, such as HPGe, are generally considered to display a nearly linear relationship for lower-energy ranges, but a polynomial relationship more accurately reproduces known energies throughout the entire range of our application. This level of precision is vital to accurately determine the energy of the observed γ rays resulting from the $^{\text{not.}}$B$(d,n\gamma)^{12}$C reaction to match to known nuclear states. The error on the determination of the channel is smaller than the marker used to depict the point; it is assumed there is no error in the associated tabulated energies [23].

V. EXPERIMENTAL RESULTS

The experimental investigation started by placing the detector behind the collimation and shielding just slightly outside the fan beam line. This measurement is done to account for the room return, radiation scattered or induced from other interactions of neutrons or γ rays with materials in the experiment facility. The deuteron beam was operated for 7000 seconds at 3.0 μA to produce the spectra shown in blue in Fig. 4.

The detector was shifted back in to the center of the beam line, 9.5 m from the boron target at the 0° LAB angle, and the accelerator was operated under the same parameters. The experimental results, shown in black in Fig. 4, were analyzed by subtracting the room return spectrum (blue) and then application of the energy calibration and analysis techniques described above producing the spectra shown in Fig. 4.

This spectrum is broken down in multiple segments to present a more detailed view of the higher energies. There are three intense γ rays below 2 MeV that appear to be orders of magnitude more prominent than the higher energies. This spectrum may be slightly misleading because it has not been corrected for the energy-dependent intrinsic efficiency nor the event losses due to the transistor reset preamplifier. Instead, this is presented to identify peak energies and compare with known nuclear states to determine the origin.

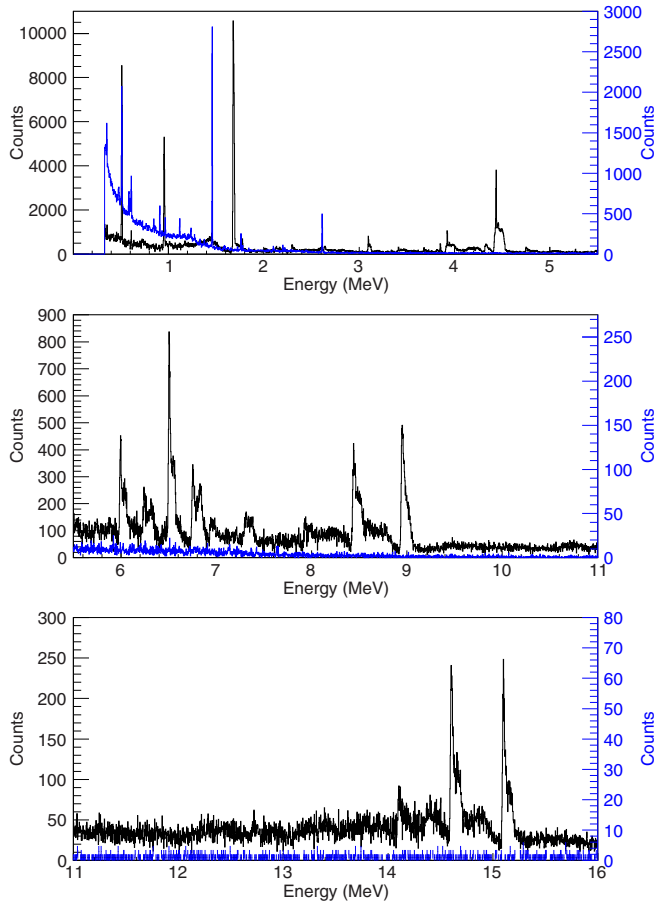

FIG. 4. High-resolution, energy-calibrated spectrum of the $^{\text{nat.}}\text{B}(d,n\gamma)^{12}\text{C}$ source using a HPGe detector.

Identifying the origin of the observed peaks is an arduous task. There are many reactions taking place that emit γ rays, but the focus here is on the largest γ-ray yields in order to determine if this source is a viable option for active interrogation applications. Many techniques were used to identify the possible origins, but some peaks may be the result of a combination. The higher-energy γ rays are generally a good indication of origin because there are not many known nuclear states to produce a specific energy within a margin of error. To determine their potential origin, we combine the superior energy resolution of the HPGe detector, high fidelity energy calibration, simulation-predicted reactions and resulting nuclei, and corresponding known nuclear states. A summary of the observed γ-ray energy and most likely origin can be seen in Table III. A more detailed explanation is given about the determination of each peak origin as it is discussed below.

The main observable reaction is the desired $^{11}\text{B}(d,n\gamma)^{12}\text{C}$ resulting in the most prominent γ-ray yields of 4.438 MeV ($2^+ \rightarrow 0^+$) and 15.1 MeV ($1^+ \rightarrow 0^+$). Some of the observed γ rays stem from secondary and tertiary reactions taking place from reactions such as $^{11}\text{B}(d,n)3\alpha$ where the α particles go on to create other nuclear reactions.

While this is not an exhaustive list of all γ lines detected, it is a list of the most prominent observed γ deexcitations taking place. Some of the features in the spectrum are omitted because they are poorly resolved. Upon analysis, they appear to be a combination of double and single escape peaks in addition to a Doppler-broadened full energy peak within a few keV of each other yielding one large feature. The uncertainty of this finding was too large to be considered definitive, and other experiments should be conducted attempting to resolve this.

TABLE III. A summary of the most intense peaks observed. Identified by the energy calibrated peak centroid and propagated uncertainty. The reactions and transitions are only some of the possible reactions emitting γ rays within the uncertainty range.

γ energy	Energy error	Reaction	Transition
511.4 keV	± 1.29 keV	β^+ annihilation	
954.3 keV	± 2.43 keV	$^{11}\text{B}(n,\gamma)^{12}\text{B}$	$2^+ \rightarrow 1^+$
		$^{11}\text{B}(d,p)^{12}\text{B}^*$	$2^+ \rightarrow 1^+$
1684.14 keV	± 1.21 keV	$^{11}\text{B}(d,\alpha)^{9}\text{Be}^*$	$\frac{1}{2}^+ \rightarrow \frac{3}{2}^-$
4437.87 keV	± 2.27 keV	$^{11}\text{B}(d,n)^{12}\text{C}^*$	$2^+ \rightarrow 0^+$
		$^{27}\text{Al}(p,p')^{27}\text{Al}^*$	$\frac{9}{2}^+ \rightarrow \frac{3}{2}^+$
4458.08 keV	± 3.02 keV	$^{27}\text{Al}(n,\gamma)^{28}\text{Al}$	$4^+ \rightarrow 3^+$
6505.46 keV	± 3.48 keV	$^{27}\text{Al}(\alpha,p)^{30}\text{Si}^*$	$5^+ \rightarrow 4^+$
		$^{27}\text{Al}(\alpha,n)^{30}\text{P}^*$	$1^- \rightarrow 0^+$
		$^{208}\text{Pb}(n,n')^{208}\text{Pb}^*$	$1^+ \rightarrow 0^+$
		$^{12}\text{C}(\alpha,n)^{15}\text{O}^*$	$\frac{5}{2}^+ \rightarrow \frac{5}{2}^+$
6756.70 keV	± 3.91 keV	$^{11}\text{B}(d,\alpha)^{9}\text{Be}^*$	$\frac{9}{2}^+ \rightarrow \frac{3}{2}^-$
8951.76 keV	± 2.18 keV	$^{27}\text{Al}(p,p')^{27}\text{Al}^*$	$\frac{9}{2}^+ \rightarrow \frac{5}{2}^+$
		$^{27}\text{Al}(n,n')^{27}\text{Al}^*$	$\frac{9}{2}^+ \rightarrow \frac{5}{2}^+$
		$^{27}\text{Al}(n,n'\alpha)^{23}\text{Na}^*$	$\frac{7}{2}^- \rightarrow \frac{5}{2}^+$
		$^{27}\text{Al}(\alpha,p)^{30}\text{Si}^*$	$2^+ \rightarrow 0^+$
15101.90 keV	± 6.80 keV	$^{11}\text{B}(d,n)^{12}\text{C}^*$	$1^+ \rightarrow 0^+$
		$^{10}\text{B}(d,\alpha)^{8}\text{Be}^*$	$1^+ \rightarrow 2^+$

Once the energies of these γ rays were determined, we searched the tabulated energy states in the Evaluated Nuclear Structure Data File (ENSDF) from the National Nuclear Data Center (NNDC) managed by Brookhaven National Lab [23] and selected possible candidates based on kinematics and available energy in the system. The γ rays emitted in span between 4.4 and 15.1 MeV can potentially be explained by numerous reactions. These peaks may originate from a combination of some or all of the possibilities listed. However, it is important to consider the possibility that these could be from a currently unknown state in one of the constituent isotopes or subsequent reaction products.

Germanium can have (n,γ) reactions leading to excess signal in the detector [24] that did not originate in the source target. To rule out γ rays produced from neutrons in the environment, we used a 50.8-cm-thick borated poly (5%) block to filter out neutrons from the reaction. Our in-beam measurements do not show any discernible peaks from neutron interactions in the Ge detector that would be expected in an environment with neutrons. Therefore, we conclude that the amount of neutrons making it to the environment is negligible.

In addition, we investigated the natural background and room return by moving the edge of the detector 2 cm outside of the beam line. We did not observe any γ-ray peaks except

natural background, ^{232}Th, and ^{40}K, as shown in blue in Fig. 4 with the exception of a 0.511 MeV peak resulting from pair production elsewhere in the room. Most importantly, there are no distinguishable peaks above the 2.614 MeV γ ray of ^{232}Th, indicating that all of the high-energy events are coming from the boron target region and not from other material in the room.

Most of the prominent γ rays observed come from the (deuteron-boron) reaction result in either excited states of beryllium, boron, or carbon. However, some of the states come from neutron interactions while propagating through the natural boron target and aluminum target holder. One of the intense low-energy lines, 0.954 MeV, comes from neutron capture in ^{11}B to an excited ^{12}B nucleus which then deexcites through γ emission. There is also a possibility that this could be caused by a $^{11}\mathrm{B}(d,p)^{12}\mathrm{B}^*$ resulting in the same 1^+ excited state of ^{12}B.

Another intense observed peak is found to be 1.684 MeV which stems from the $^{11}\mathrm{B}(d,\alpha)^{9}\mathrm{Be}$ reaction predicted by the GEANT4 simulations to occur in approximately 6.2% of the deuteron interactions. The intensity of this peak relative to the high-energy peaks may be misleading on the graphical representation of the spectrum, Fig. 4, because we make no correction for detector efficiency in order to preserve the integrity of the data. As mentioned before, the operation of this particular setup makes the detection efficiency convoluted because it is not just a function of interaction probability as is the case with most detectors. This detector has an efficiency loss at high energies due to the energy-deposition rate.

The two main energies between the well-understood 4.4 and 15.1 MeV lines were found to result from subsequent nuclear reactions in the aluminum target holder and endcap. These lines were calculated to be 6.505 and 8.951 MeV. Matching these to known nuclear states within the error of the energy calibration, we determine the most probable origin to be in the aluminum holder resulting from proton and α-particle interaction with the ^{27}Al. Aluminum is typically used in these types of experiments due to the low neutron interaction cross sections at low neutron energies. However, here we have an abundance of neutrons averaging 6.75 MeV and ranging up to 16.53 MeV, as shown in Fig. 1.

Inspecting published cross sections for aluminum, we find significant probability of (n,p) and (n,α) reactions with neutrons above about 3 MeV. Previous work has estimated the neutron production from the $^{11}\mathrm{B}(d,n)^{12}\mathrm{C}$ to be approximately two orders of magnitude greater than that of the γ rays [22]. These peaks could have minor contributions from the room environment or the collimation itself, but the solid angle is small, making it improbable. For example, ^{23}Na does have some transitions that emit γ rays within the calculated error of the observed line. This could be from interactions in the large concrete collimators used in the shielding; however, it would have to be coming from the faces of the collimators and emitted in an extremely small solid angle to reach the detector 6 m away. These γ rays were not observed when the detector was moved slightly out of the collimated beam line.

The most difficult reaction to determine is the origin of the 6.5 MeV γ ray. This can be the result of multiple reactions; we have listed a few in Table III. The boron target is essentially surrounded by aluminum and steel as structural components and lead as shielding, so these reactions are highly probable given the plethora of particles in the area. A transition in ^{15}O may be responsible for some of this emission because the observed energy precisely matches the published γ-ray energy of 6.505 MeV [23]. The deuteron beam impacting the target is about 1 cm^2 and operates at roughly 20 μA of beam current, which translates to approximately 1.6×10^{14} deuterons per second incident on a small surface area. Over time, transmutation of the target can play a large role because there will be a buildup of beryllium, carbon, and trapped nitrogen in the atomic lattice structure of the boron target. The current target is roughly two years old at the time of this study, which allows time for significant in-growth of these atoms in the material. The stated reaction, $^{12}\mathrm{C}(\alpha,n)^{15}\mathrm{O}$ is just one possibility to reach this state of ^{15}O. We are possibly observing part of the CNO cycle given the abundance of charges particles in the target area.

A small contribution to the 15.1 MeV peak could stem from the Hoyle state of carbon through the $^{10}\mathrm{B}(d,\alpha)^{8}\mathrm{Be}^*$ reaction resulting in a brief ^{12}C formation then α decay to the excited ^{8}Be nucleus resulting in a γ transition from $1^+ \rightarrow 2^+$. This cannot be verified solely with the γ-ray observation method we are employing, but it is energetically possible and predicted by the simulation as well. The observed spectrum does show signs of other γ rays from an excited ^{8}Be nucleus, such as the 3.03 MeV γ ray.

Throughout the studies conducted as part of this work, there has always been an intense 0.511 MeV emission from the target. Routine safety surveys upon entry to the accelerator area require the use of an ion chamber to ensure that the accelerator is off. These surveys lead to another important observation that the target was still emitting fairly intense radiation for a period of time after shutting down the beam. Studies of this γ radiation led to findings of activation products such as the 1.79 MeV from aluminum and a highly intense 0.511 MeV emission.

The 0.511 MeV γ ray stems from annihilation, meaning the parent decay product must be a positron (β^+) emitter; thus, the parent isotope has an excess of protons. This is usually a very unstable configuration leading to short half-lives, on the order of a few seconds or less; however, this emission lasted for more than an hour. This was investigated by employing a LaBr detector in the beam line using the list mode capabilities of the CAEN DT5730 digitizer where each event is saved with a time stamp. The deuteron beam was operated at 20 μA for 30 minutes to build up the decay products in the $^{\mathrm{nat.}}$B target. Data acquisition started a few seconds before the beam was shut off and continued for a total of 1800 seconds. The 0.511 MeV events were isolated and plotted as events per second producing the activation die-away plot shown in Fig. 5.

The first 200 seconds of the decay radiation are ignored since there will likely be an abundance of short-lived positron emitters. The main interest here is the most prominent decay products, which are also long lived. The slope of the decay curve was analyzed and fit with a single exponential decay function, Eq. (1), using ROOT in efforts to determine the

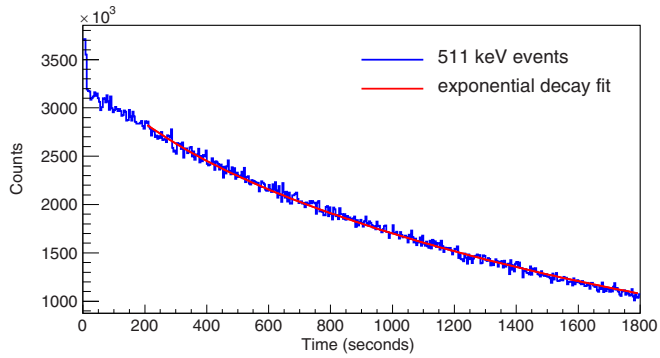

FIG. 5. Isolated 0.511 MeV activation product decay from the target immediately after shutting off the beam. The red line denotes a fitted relationship of Eq. (1).

decay constant λ, which contains the half-life $t_{1/2}$:

$$\sum_i N_i = \sum_i N_{0_i} e^{-\lambda_i t}. \quad (1)$$

Inspecting the predicted nuclei resulting from the nuclear reaction simulations in the target, there is only one proton heavy isotope produced in large quantities with a half-life on this order of magnitude, ^{11}C. This is a known β^+ emitter with a tabulated half-life of 1221.8 seconds [23]. Fitting this equation to two isotopes, and using the ^{11}C half-life as an initial condition, the unknown half-life is calculated to be 148.93 seconds. This closely matches the half-life of ^{30}P which is a predicted product of the aluminum-neutron simulations conducted as part of this investigation. This simulation also predicts a buildup of ^{30}S, another β^+ emitter, which has a short half-life of 1.178 seconds and decays into the longer-lived ^{30}P. This is an important finding that lends validity to the simplified simulation but also because both ^{30}P and ^{30}S have multiple γ emission possible in the 6.5 MeV range that could also be adding to the observed spectrum.

The ^{11}C buildup and decay presents another interesting relationship because it is generated from deuteron-on-^{10}B reactions. It decays to form ^{11}B which then undergoes any of the listed reactions that may produce the desired γ rays previously described. This is akin to a breed-and-burn cycle used in nuclear reactors with uranium and plutonium isotopes.

VI. CONCLUSIONS

Our investigation into the γ rays produced from the low-energy nuclear reaction, $^{\text{nat.}}$B$(d,n\gamma)^{12}$C, using a specialized HPGe resulted in the first high-resolution γ-ray spectrum of this reaction. We are able to determine and tabulate the observed γ-ray energies with confidence and determine that they originate in the boron target or adjacent structural components of the accelerator. Ruling out room return and knowing the exact emission energies, we can conclude that this is a viable source to use for nuclear security applications, especially active interrogation and photofission techniques.

ACKNOWLEDGMENTS

The authors gratefully acknowledge the support from the National Science Foundation under Grant No. ECCS-1348366 and by the U.S. Department of Homeland Security under Grant No. 2014-DN-077-ARI079-02. The views and conclusions contained in this document are those of the authors and should not be interpreted as necessarily representing the official policies, either expressed or implied, of the U.S. Department of Homeland Security. We are grateful to Peter Binns of MIT Bates Linear Accelerator Center for help with operating the linear accelerator.

Special thanks to Dr. John Wood, physicist at Georgia Tech, for discussion around potential nuclear states. Also, thanks to the ARCS foundation for support and recognition and continued dedication to college scientists in STEM fields.

[1] V. R. Johnson, Phys. Rev. **86**, 302 (1952).
[2] D. Cohen, B. J. Moyer, H. Shaw, and C. Waddell, Phys. Rev. **96**, 714 (1954).
[3] J. B. Marion, T. W. Bonner, and C. F. Cook, Phys. Rev. **100**, 91 (1955).
[4] R. W. Kavanagh and C. A. Barnes, Phys. Rev. **112**, 503 (1958).
[5] H.-M. Kuan, P. R. Almond, G. Din, and T. Bonner, Nucl. Phys. **60**, 509 (1964).
[6] E. Almqvist, D. A. Bromley, A. J. Ferguson, H. E. Gove, and A. E. Litherland, Phys. Rev. **114**, 1040 (1959).
[7] C. A. Diget, F. C. Barker, M. J. G. Borge, R. Boutami, P. Dendooven, T. Eronen, S. P. Fox, B. R. Fulton, H. O. U. Fynbo, J. Huikari, S. Hyldegaard, H. B. Jeppesen, A. Jokinen, B. Jonson, A. Kankainen, I. Moore, A. Nieminen, G. Nyman, H. Penttilä, V. F. E. Pucknell, K. Riisager, S. Rinta-Antila, O. Tengblad, Y. Wang, K. Wilhelmsen, and J. Äystö, Phys. Rev. C **80**, 034316 (2009).
[8] J. Kelley, J. Purcell, and C. Sheu, Nucl. Phys. A **968**, 71 (2017).
[9] T. Taddeucci and R. Sheffield, *Neutron and Gamma-Ray Production with Low-Energy Beams*, Tech. Rep. LA-UR-07-2724 (Los Alamos National Laboratory, Los Alamos, New Mexico, USA, 2007).
[10] K. W. Cooper, T. N. Massey, and D. C. Ingram, AIP Conf. Proc. **1525**, 709 (2013).
[11] K. W. Cooper, T. N. Massey, D. Carter, and D. C. Ingram, Nucl. Instrum. Methods Phys. Res., Sect. B **305**, 45 (2013).
[12] B. J. Micklich and D. L. Smith, Nucl. Instrum. Methods Phys. Res., Sect. B **241**, 782 (2005).
[13] D. H. Morse, A. J. Antolak, and B. L. Doyle, Nucl. Instrum. Methods Phys. Res., Sect. B **261**, 378 (2007).
[14] R. C. Runkle, L. E. Smith, and A. J. Peurrung, J. Appl. Phys. **106**, 041101 (2009).
[15] R. C. Runkle, D. L. Chichester, and S. J. Thompson, Nucl. Instrum. Methods Phys. Res., Sect. A **663**, 75 (2012).

[16] S. Fetter *et al.*, Sci. Glob. Secur. **1**, 225 (1990).
[17] S. Agostinelli, Nucl. Instrum. Methods Phys. Res., Sect. A **506**, 250 (2003).
[18] J. Allison *et al.*, IEEE Trans. Nucl. Sci. **53**, 270 (2006).
[19] L. Desorgher (private communication).
[20] D. Wright (private communication).
[21] P. B. Rose, Jr., Ph.D. thesis, Georgia Institute of Technology, 2017.
[22] P. B. Rose, A. S. Erickson, M. Mayer, J. Nattress, and I. Jovanovic, Sci. Rep. **6**, 24388 (2016).
[23] M. R. Bhat, *Evaluated Nuclear Structure Data File (ENSDF)*, Nuclear Data for Science and Technology, edited by S. M. Qaim (Springer-Verlag, Berlin, 1992), p. 817.
[24] G. Fehrenbacher, R. Meckbach, and H. G. Paretzke, Nucl. Instrum. Methods Phys. Res., Sect. A **372**, 239 (1996).